Crack Growth in a Welded Microalloyed Steel under Sulfide Stress Cracking Conditions

J.L. Albarran, H.F. Lopez, and L. Martinez

(Submitted 27 August 1997; in revised form 18 August 1998)

In this work, the hydrogen sulfide stress-corrosion cracking (SSC) susceptibility of a welded API X-80 pipeline was investigated. For this purpose, steel welding was carried out normal to the rolling direction using a 60° single V-joint design. After welding, compact modified-wedge opening loading (M-WOL) fracture mechanics specimens were machined and loaded to an applied stress intensity factor, K_I, of 27 to 53 MPa$\sqrt{m}$. This was followed by specimen exposure to H_2S saturated synthetic seawater. Each of the M-WOL specimens contained the typical microstructures developed during welding, such as the weld metal (WM), base metal (BM), and heat affected zone (HAZ). No attempt was made to establish a unique K_{ISCC} for crack arrest because its significance was not clear. Qualitatively, the experimental outcome indicated that in mode I loading under a K_I of 40.3 MPa$\sqrt{m}$ only the base metal region underwent SSC. Apparently, active anodic dissolution of the crack tip started the growth process, but it was followed by a transition to hydrogen induced cracking. At an applied K_I of 55 MPa$\sqrt{m}$ and under similar exposure times, crack growth in the base metal was discontinuous and tended to follow the grain boundaries. Moreover, the HAZ exhibited the least SSC susceptibility as inferred from the relatively short crack propagation lengths (0.829 mm). In this case, it was found that the crack path was highly tortuous due to the presence of acicular ferrite and a refined grain structure. The most SSC susceptible condition was found in the weld metal where crack lengths of up to 4.2 mm developed. In this case, the presence of a relatively coarse dendritic structure coupled with interdendritic segregation provided a weak path for crack propagation.

Keywords crack formation, microalloyed steel, microstructure, sour gas environment, stress-corrosion cracking

1. Introduction

Hydrogen sulfide stress-corrosion cracking (SSC) is a widely known phenomenon that often leads to failure in pipelines for oil transmission, as well as in other oil field facilities. In general, this mode of degradation has been attributed to the production of nascent hydrogen as H_2S reacts with the steel to form an FeS film and nascent hydrogen. Apparently, the hydrogen thus produced is unable to effectively recombine into gaseous H_2 and tends to be absorbed in the metal in regions of high internal stresses of tensile nature (Ref 1). In relatively large oil field installations, it is expected that welded structural components will eventually come into contact with sour (H_2S) gas environments. Hence, the performance of welded joints under H_2S conditions needs to be closely monitored in order to incorporate it in the design of welded structures.

In high-strength low-alloy (HSLA) steels exposed to sour gas environments, SSC usually occurs by the combination of a susceptible microstructure and the presence of tensile stresses (Ref 2). Alternatively, in stress-free pipelines exposed to sour environments, hydrogen embrittlement also known as hydrogen induced cracking (HIC) is known to take place (Ref 3, 4). Accordingly, in order to reduce the potential for environmental cracking, the National Association of Corrosion Engineers (NACE) has developed a series of guidelines (Ref 5), such as the NACE TM 0177-90 and NACE MR 0175-92, to ensure acceptable materials performance under SSC environments. In particular, maximum yield strengths of 690 MPa (Ref 3) or hardness of 22 HRC (Ref 5) have been established as limiting in low-alloy steels. Nevertheless, the NACE standards have limited applicability in ranking the new grades of corrosion-resistant alloys for service in sour environments (Ref 6).

The relative SSC susceptibility of HSLA steels is strongly influenced by heat treating (Ref 7, 8), as well as the alloy composition and the presence of residual elements (Ref 9, 10). In particular, nonmetallic inclusions, grain boundary segregates, precipitates, and hard bands all seem to influence the overall steel susceptibility (Ref 11).

The SSC susceptibility of HSLA steels is expected to be further increased in welded regions due to the presence of nonequilibrium phases, segregation bands, and internal/residual stresses (Ref 12). It has been reported (Ref 8) that sour gas susceptibility increases at high weld strengths or hardness values, residual stresses promote SCC cracking in the weld metal-HAZ regions exposed to sour environments, and welding electrodes with more than 1 wt% Ni are to be avoided to minimize SSC.

As a result, preheat and postheat welding treatments are often used to reduce the effect of internal/residual stresses, as well as the weld hardness. The work of Fraser and Metzbower (Ref 13) indicates that the development of cracks in the welded regions is strongly influenced by the resultant welding microstructures, induced defects, and residual stresses. In addition, Onsoien et al. (Ref 8) found that the SSC resistance of welded

J.L. Albarran and **L. Martinez,** Laboratorio de Cuernavaca, Instituto de Fisica, UNAM, Apdo. Postal 48-3, C.P. 62251, Cuernavaca, Morelos, Mexico; **H.F. Lopez,** Materials Department, College of Engineering and Applied Science, University of Wisconsin-Milwaukee, P.O. Box 784, Milwaukee, WI, 53201. Contact H.F. Lopez at e-mail hlopez@csd.uwm.edu.

plates can be improved by slow cooling after welding. Apparently, slow cooling rates promote the formation of a ferritic Widmanstatten structure. Under these conditions, the SCC threshold stresses are significantly increased up to 60 to 70% of the yield strength (Ref 8). Moreover, crack propagation can be rate controlled by either preferential grain boundary dissolution and repetitive film rupture (Ref 10) or by successive events related to microcrack nucleation and linkage ahead of the main crack tip (Ref 14).

Nevertheless, further work is needed to disclose the active microcracking mechanisms as a function of the sour environment, state of stresses, and welded microstructures (Ref 7, 15). The present work further examines the performance of welded pipeline steel exposed to SSC environments. In particular, it investigates the relative susceptibilities exhibited by the various microstructures developed in the welded regions, as well as the base metal (BM).

2. Experimental Procedure

The material used in this study was microalloyed pipeline steel API X-80, under the API 5XL standard. Table 1 gives the chemical composition of the steel plate and the weld metal (WM). Welding was accomplished by manual arc welding, in the direction normal to the rolling plane, using a 60 ° single-V joint design (Fig. 1a). Before welding, the electrodes were annealed at 430 °C, and the steel plate preheated at 200 °C. Figure 1(b) shows the experimental setup involving the steel plates to be welded. The root pass was overlaid at 10 mm/s at 175 A. Subsequent filler passes were overlaid at 7 mm/s and 175 A, whereas the cap layer was placed at 4 mm/s and 150 A. After welding, the plate was annealed at 400 °C for 1 h and then cooled in still air following the API 1104 recommendations (Ref 16). Cross sections of the welded plate were then cut and polished for metallographic observations and microhardness profile measurements across the base metal, weld metal, and HAZ regions.

Modified wedge opening loading (M-WOL) (Ref 17) samples were machined from the welded plates containing both sides of the weld metal. Figure 2(a) shows schematically the M-WOL specimen dimensions, as well as the specimen layout in the welded plate (Fig. 2b). The specimens were artificially notched using a spark machine with copper wire to avoid the buildup of internal stresses and work hardening of the crack tip due to fatigue precracking. In addition, the specimens were loaded at a stress intensity factor K_I of 30 MPa$\sqrt{m}$ and then exposed to the sour media until a crack was generated. At this time, the specimens were removed from the sour aqueous solution. This was done in order to minimize the effect of the re-

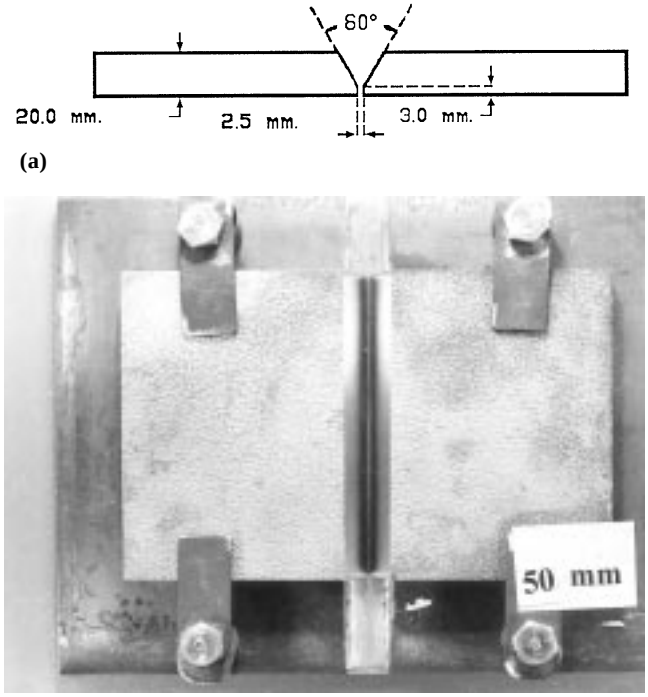

Fig. 1 (a) Single V-joint design for welding. (b) Experimental arrangement for the welding procedure

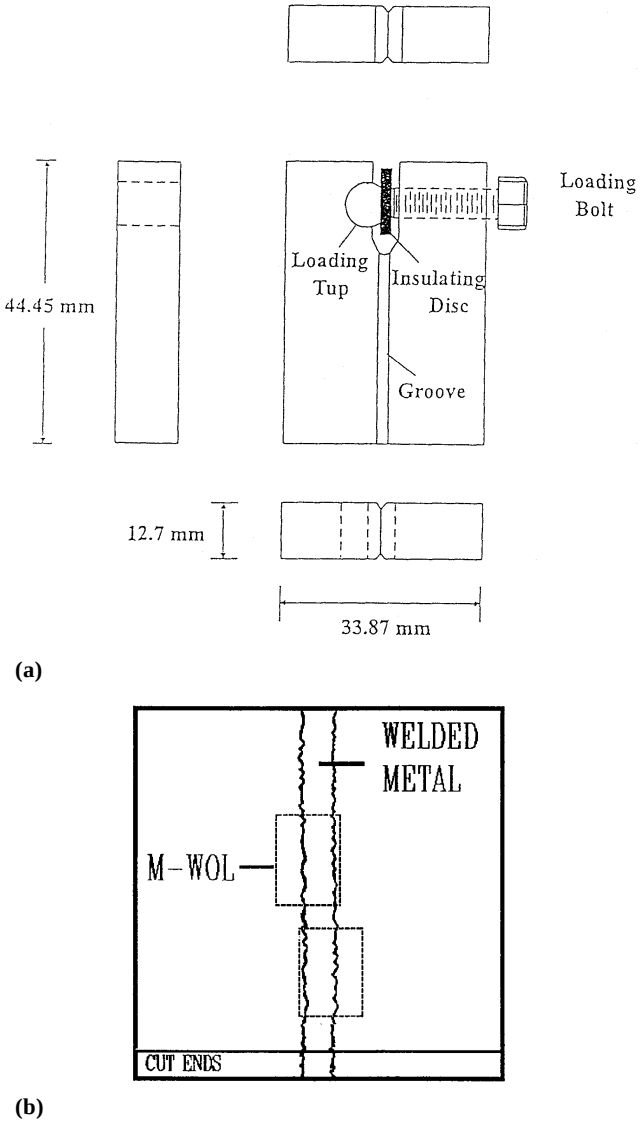

Fig. 2 (a) Geometry and dimensions of M-WOL samples. (b) Layout of the samples taken from the welded plate

melted surface layer on the SSC susceptibility of the steel. The specimens were then loaded to three different values of K_I: 26.7, 40.3, and 52.4 MPa$\sqrt{m}$. The back-face strain technique (Ref 18) was employed in order to measure the applied K_I. The self-loaded M-WOL specimens were then placed back in the synthetic seawater solution (ASTM D 1141) saturated with H_2S at a pH of 4 in a glass vessel at room temperature. Crack growth was systematically monitored at 12 hour intervals. At the end of each test, the composition of the corrosion products was analyzed in a JEOL model 6400 scanning electron microscope (SEM) equipped with a Noran microprobe type Norvar used for the detection of light elements. The SEM uses a turbo pump and cold traps to avoid carbon from the oil to reach the detector. Peaks corresponding to oxygen, as well as the other element, were automatically identified by the software and hardware in the Voyager (National Computer Technology, Inc., Sacramento, CA) computer system.

3. Results and Discussion

3.1 Microstructure

Figure 3(a) is a macrograph of the welded plate containing the BM, HAZ, and WM regions. Notice that the HAZ extends for approximately 2 mm. Figure 3(b) shows the microhardness profiles developed across the welded plate. Maximum hardness values of 300 kg/mm^2 were found in the HAZ at the root pass location, but they decreased to 270 kg/mm^2 near the region adjacent to the last filler pass. The weld metal exhibited the lowest hardness values as a result of stress relieving through alloy reheating induced by previous filler passes. Table 2 shows the experimental conditions and data obtained on the SSC susceptibility of the specimens exposed to the sour environment, including average crack lengths. No attempt was made to establish specific K_{ISSC} values, because the various weld regions were involved, each of which possesses a different microstructure, state of internal/residual stresses, and SSC susceptibilities. In addition, the NACE standard TM0177-90 does not allow these tests as valid for K_{ISSC} measurements. Nevertheless, the experimental outcome qualitatively provides valuable information on the relative susceptibilities of each of the welded microstructures.

From Table 2, it can be observed that the specimens loaded at a K_I of 26.7 MPa$\sqrt{m}$ did not exhibit crack propagation when exposed to the sour environment for 720 h. In this case, conditions for favorable crack growth did not develop, despite the fact that the HAZ or WM hardness was higher than the 22 HRC proposed limit to avoid SSC. Apparently, the applied K_I was somewhat below the critical K_{ISSC} needed to promote crack

Table 1 Chemical composition of the API X-80 steel plate and of the weld metal

	Composition, wt%													
Material	**C**	**Si**	**Mn**	**P**	**S**	**Al**	**Ni**	**Cr**	**Mo**	**V**	**W**	**Nb**	**Cu**	**Ti**
X-80	0.13	0.20	1.52	.009	.009	.028	0.21	0.11	0.05	0.1	.005	.038	.025	.005
Weld metal	0.38	0.20	0.60	…	…	…	…	0.60	…	…	…	…	…	…

Table 2 Experimental conditions and crack lengths in specimens exposed to the sour solution

Specimen	**K_1 initial, MPa$\sqrt{m}$**	**a_{arrest} in base metal, mm**	**a_{arrest} in HAZ, mm**	**a_{arrest} in welded metal, mm**	**Time of test, h**
S_1	26.7	…	…	…	720
S_2	40.3	1.044	…	…	336
S_3	52.4	2.622	0.829	4.195	24

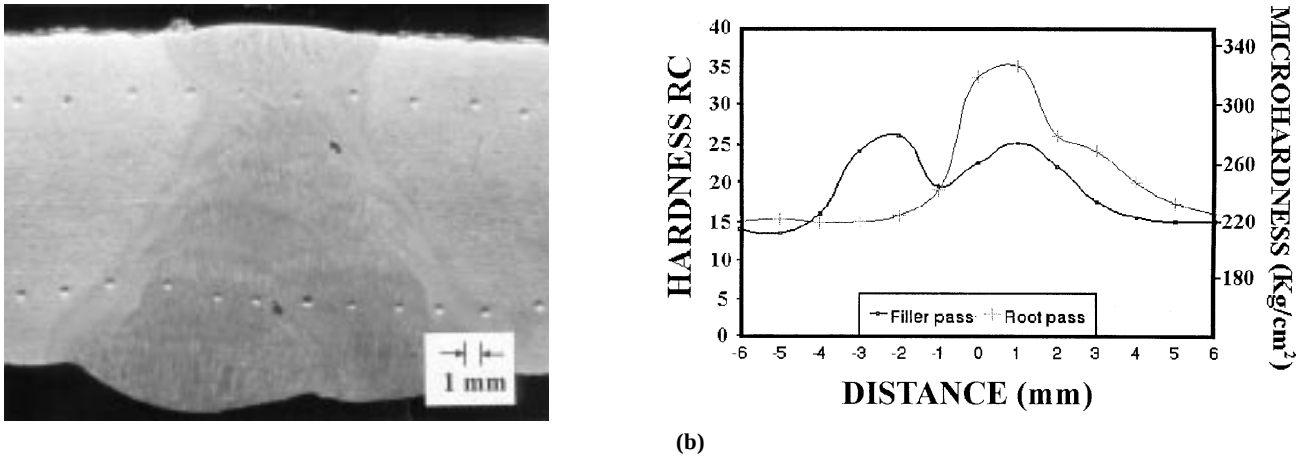

(a) **(b)**

Fig. 3 (a) Macrograph of the welded plate. (b) Hardness profiles across the welded regions (BM, HAZ, and WM)

growth in any of the microstructures developed. This in turn agrees with previous reports (Ref 14) of K_{ISSC} values about 26 MPa$\sqrt{m}$ for the same steel that are close to the applied K_I.

In the particular specimen configuration, all of the various microstructures were present across the specimen thickness and exposed to the same applied K_I. Hence, the relative SSC susceptibilities of the welded regions can be directly related to the exhibited crack propagation lengths for a given exposure time. Accordingly, the HAZ seemed to exhibit the least SSC susceptibility under all the applied K_I, whereas the weld metal became highly susceptible to SSC at applied K_I values of 52.4 MPa$\sqrt{m}$.

Figure 4 (a to d) shows the various microstructural features developed in the base metal, HAZ, and weld metal. The base metal region adjacent to the HAZ consisted mainly of a mixture of equiaxed ferrite and pearlite bands with partial recrystallization near the HAZ (Fig. 4b). The HAZ next to the base metal region shows ferrite sideplates with partially recrystallized

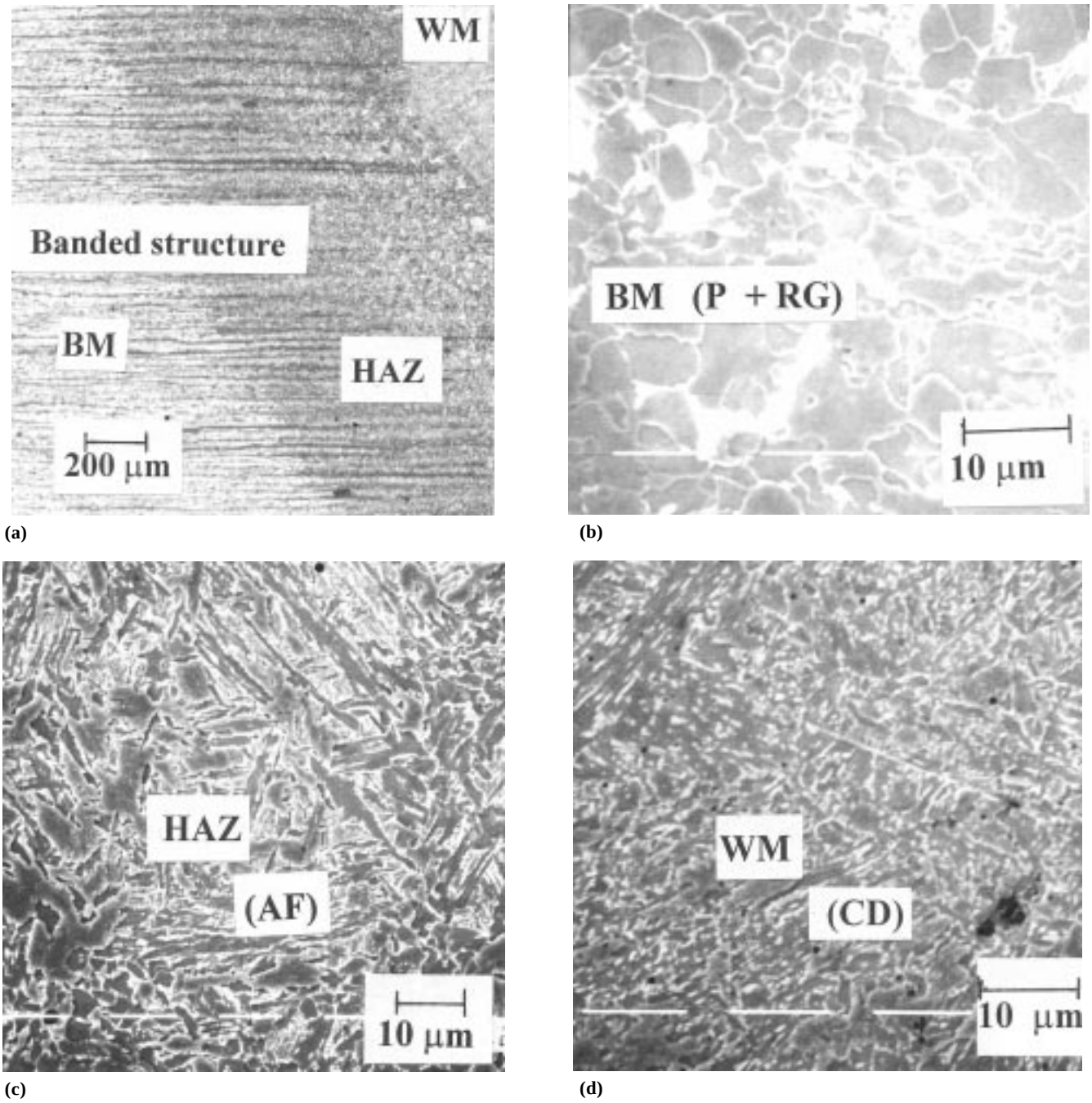

Fig. 4 (a) Micrograph of the welded plate showing the various microstructures developed. (b) Microstructure of the BM next to the HAZ consisting of partially recrystallized grains and pearlite regions (P + RG). (c) Acicular ferrite found in the HAZ near the WM region. (d) Coarse dendritic (CD) structure corresponding to the WM

regions (i.e., grain sizes <10 μm) and grain coarsening near the weld metal regions (Fig. 4c). The weld metal developed a typical dendritic grain structure with a network of small subgrains (Fig. 4d). In addition, the weld metal exhibited some degree of porosity probably as a result of gas entrapment during welding.

At intermediate K_I of 40.3 MPa$\sqrt{m}$, crack growth was only exhibited in the base metal regions. The resultant crack path produced in this microstructure (specimen S_2) is shown in Fig. 5(a). Notice the development of crack branching with preferential growth along the ferritic bands. Experimentally, it was found that in this case, crack initiation is closely related to preferential alloy dissolution along grain boundaries as described in detail elsewhere (Ref 19, 20). An analysis of the corrosion products found within the early crack (see arrow in Fig. 5b) indicated the presence of significant amounts of sulfur, oxygen, and iron. However, as the crack evolved further, a transition to discontinuous crack growth presumable by hydrogen embrittlement developed ahead of the main crack (~80 μm from main crack tip). In particular, the deeper cracks did not contain sulfur or oxygen.

At an applied K_I of 52.4 MPa$\sqrt{m}$, crack growth was found to take place in all of the weld regions. Under these conditions, there was a lack of preferential dissolution in the base metal region. Instead, discontinuous crack growth was dominant from the very beginning. Apparently, crack propagation was somewhat similar to that found in the specimen S_2, with preferential growth along the grain boundaries (see Fig. 6a).

Figure 7(a) shows the crack development in the HAZ, where the crack tends to move away from the ferritic Widmanstatten structure and into the partially recrystallized grains (HAZ/BM interface). In particular, it was found that the crack avoided growing into the acicular ferrite grain structure (HAZ). Microstructurally, the crack path consists of a mixture of intergranular and transgranular components in the partially recrystallized BM grain structure (Fig. 7b). The lack of crack propagation into the acicular ferritic microstructure can be explained by the observations of Onsoien et al. (Ref 8). In their work, they found that the SSC resistance of welded joints is significantly improved by using cooling rates that promote the formation of ferrite side plates.

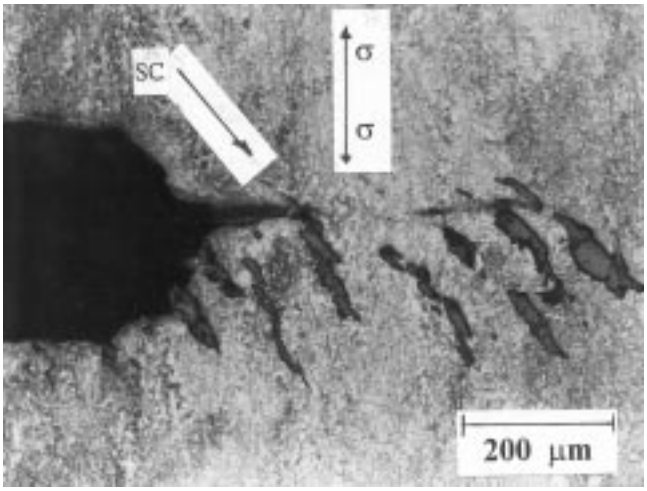

(a)

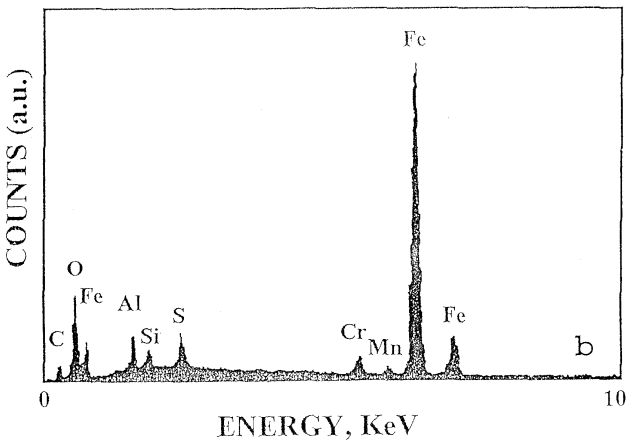

(b)

Fig. 5 (a) Crack growth path in the BM (specimen S_2). (b) EDX profile of elements found in the starting crack

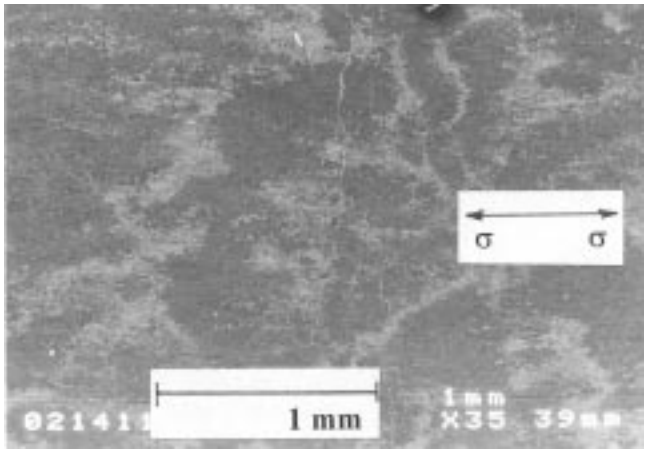

(a)

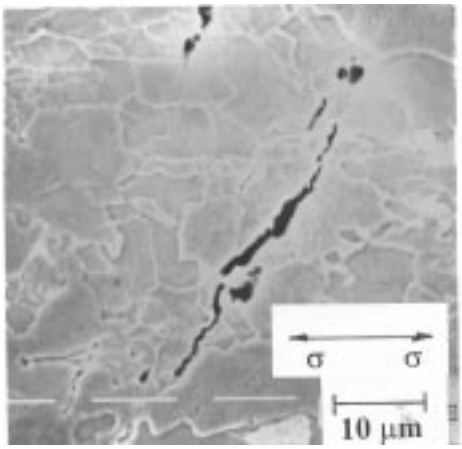

(b)

Fig. 6 (a) Crack growth path in the BM (specimen S_3). (b) Detail of the path followed by the crack ahead of the main crack tip

3.2 Weld Metal

In the weld metal regions, the welding process refines and partly removes the dendritic matrix developed as a result of metal reheating during subsequent filler passes. Even though the weld metal exhibits only a minimal SSC susceptibility in specimens tested at applied K_I below 40 MPa$\sqrt{m}$, it becomes highly embrittled under an applied K_I of 52.4 MPa$\sqrt{m}$ (specimen S_3). Figure 8(a) shows the crack path followed in the weld metal regions. In particular, the crack tends to follow the dendritic boundaries that are decorated with carbides as shown in Fig. 8(b). Segregation of impurities to the dendritic boundaries also contributes to the crack path resulting in a stepwise mode of cracking. In addition, the crack tends to move toward the central region of the weld metal where the dendritic grains are relatively coarse (Fig. 8b). It is likely that the combination of relatively large dendritic grains coupled with significant interdendritic segregation provides a weak path for SSC crack growth.

The conditions for crack growth in sour environments can be described by a critical condition that is a function of the combination of three factors: potential crack path for a given microstructure, state of internal and external stresses, and hydrogen concentration in front of the crack tip. Hence, under similar environments and applied stresses, the dominant factors are essentially microstructural. Accordingly, the potential crack path will be provided by those microstructural features that require the least elastic energy to promote bond breaking in the presence of hydrogen. This agrees with the experimental observations of crack shifting toward regions where there are less obstacles for crack propagation (Fig. 5 and 8), or along interdendritic regions where grain boundary segregation and a continuous interface are likely to be present, such as the weld metal regions. In addition, residual stresses can effectively reduce the critical condition for crack growth promoting crack shifting toward the BM/HAZ regions (Fig. 5).

Finally, the outcome of the present work indicates that under similar sour gas environments and applied K_I, the performance of the welded plate is strongly influenced by the resultant microstructures and internal state of stresses. As a general rule, crack growth under SSC conditions will occur whenever a susceptible path is present in the welded steel. This in turn can be described by the applied K_I being in excess of the intrinsic K_{ISSC} needed for crack propagation into a given microstructure.

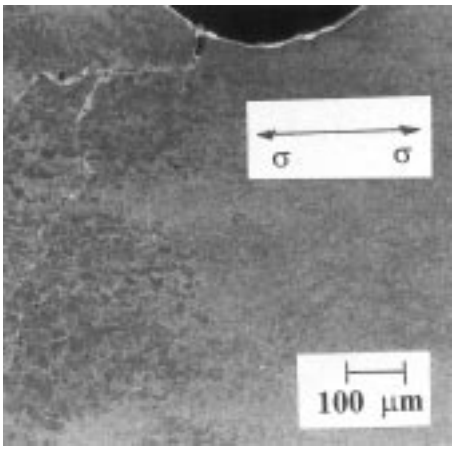

(a)

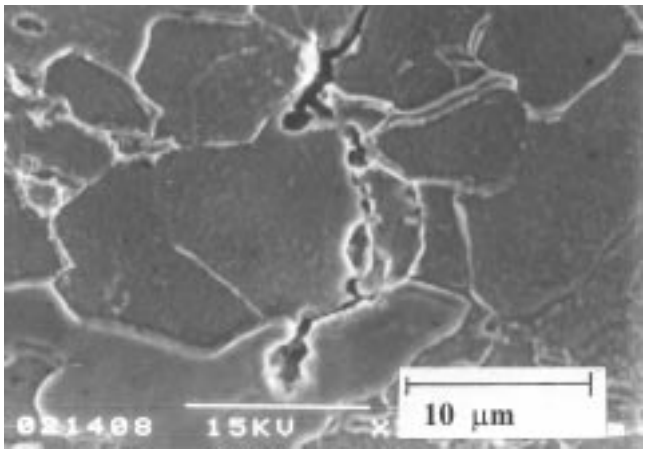

(b)

Fig. 7 (a) Crack path observed in the HAZ. (b) Detail of the crack path developed in front of the main crack tip

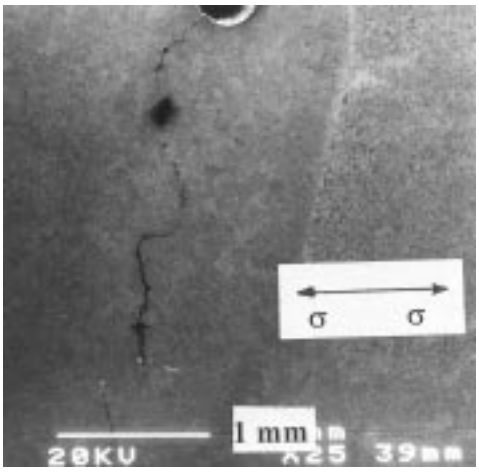

(a)

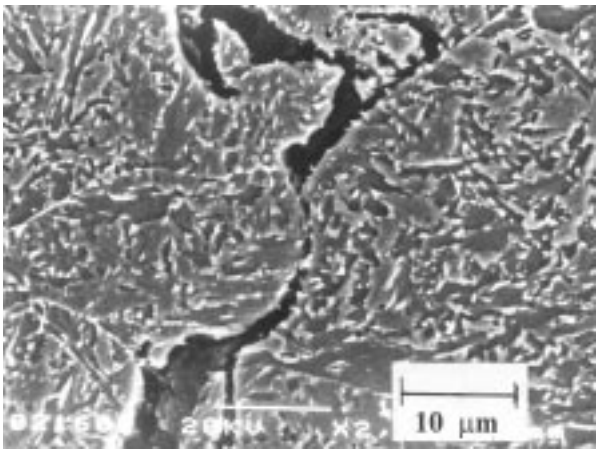

(b)

Fig. 8 (a) Stepwise cracking exhibited by the WM. (b) Detail of the crack path followed in the WM

4. Summary

The sour gas resistance of welded joints was investigated using self-loaded M-WOL specimens containing the base metal (BM), heat affected zone (HAZ), and weld metal (WM) regions. It was found that specimen exposure to the sour environment for 336 h under an applied K_I of 40.3 MPa$\sqrt{m}$ led to SSC only in the base metal region. At an applied K_I of 53 MPa$\sqrt{m}$ and under similar exposure times, crack growth was observed in all the welded conditions. Under these conditions, SSC in the base metal was discontinuous and closely related to the nucleation of microcracks and voids along the grain boundaries reflecting typical hydrogen embrittlement conditions. The most SSC susceptible condition was found in the weld metal where crack lengths of up to 4.2 mm developed. In this case, the presence of a relatively coarse dendritic structure coupled with interdendritic segregation provided a weak path for crack propagation. The HAZ exhibited the highest SSC resistance as inferred from the relatively short crack propagation lengths (0.829 mm). In this case, it was found that the crack path was highly tortuous due to the presence of a matrix consisting of acicular ferrite.

Acknowledgments

The authors thank the following people for their technical support: Anselmo Gonzalez, Osvaldo Flores, and Rene Guardian. This work was partially supported by PADEP-UNAM, grant 05301. Also, the support provided through the DGPA-UNAM grant IN105997 is greatly acknowledged. The support provided by the National Science Foundation under contract NSF-INT-9314175 for Professor Hugo F. Lopez is gratefully acknowledged.

References

1. H.K. Birnbaum, Mechanisms of Hydrogen-Related Fracture of Metals, *Environment-Induced Cracking of Metals*, R.P. Gangloff and M.B. Ives, Ed., National Association of Corrosion Engineers, 1990, p 21-29
2. Y. Nakai, H. Kurahashi, T. Emi, and O. Haida, *Trans. Iron Steel Inst. Jpn.*, Vol 19 (No. 7), 1979, p 401-410
3. R.S. Tresseder, *Stress Corrosion Cracking and Hydrogen Embrittlement of Iron Base Alloys*, R.W. Stahle, J. Hochman, R.D. McCrigth, and J.E. Slater, Ed., National Association of Corrosion Engineers, 1977, p 147-161
4. H. Margot-Marette, G. Bardou, and J.C. Carbonier, *Corros. Sci.*, Vol 27 (No. 10/11), 1987, p 1009-1026
5. H. Buist, E. Feldhusen, and B. Fatseas, Ed., Test Methods and Material Requirements, *NACE 1992 Book of Standards*, Vol 2, National Association of Corrosion Engineers, 1992
6. Working Party on Corrosion in the Oil and Gas Industry; European Federation for Corrosion, EFC O&G 93-2 Draft 02, 1994
7. C. Christensen, *Corros. Sci.*, Vol 47 (No. 10/11), 1987, p 1137-1144
8. M.I. Onsoien, O.M. Akelsen, O. Grong, and P.E. Kvaale, *Weld. J.*, Vol 69 (No. 1), 1990, p 45-51
9. R.N. Parkins, *Fundamental Aspects of Stress Corrosion Cracking*, R.W. Staehle, A.J. Forty, and D. Van Rooyen, National Association of Corrosion Engineers, 1969, p 361
10. R.N. Parkins, Mechanisms of SCC, *Corrosion*, L.L. Shreir, Ed., Newnes-Butterworth, 1970
11. R.N. Parkins, Localized Corrosion and Crack Initiation, *Mater. Sci. Eng. A*, Vol 103, 1988, p 143-156
12. N.J. Smith, J.T. McGrath, J.A. Gianetto, and R.F. Orr, *Weld. J.*, Vol 68 (No. 3), 1989, p 112/s-120/s
13. F.W. Fraser and E.A. Metzbower, *Weld. J.*, Vol 61 (No. 4), 1982, p 112-s
14. H.F. Lopez, R. Raghunath, J.L. Albarran, and L. Martinez, *Metall. Mater. Trans. A*, Vol 27, 1996, p 3601-3611
15. J.M. Sykes, Composition, Microstructure, and Stress Corrosion Cracking, *J. Min. Met. Mater.*, Vol 45 (No. 9), 1993, p 31-35
16. API Standard 1104, Welding of Pipelines and Related Facilities, American Petroleum Institute, 1988
17. S.R. Novak and S.T. Rolfe, *Corrosion*, Vol 4, 1969, p 701
18. W.F. Deans and C.E. Richards, *J. Test. Eval.*, Vol 7, 1979, p 147-154
19. H.F. Lopez, B. Bharadwaj, J.L. Albarran, and L. Martinez, The Role of Heat Treating on the Sour Gas Resistance of an X-80 Steel for Oil and Gas Transport, to be published in *Metall. Mater. Trans. A*
20. J.L. Albarran, L. Martinez, and H.F. Lopez, The Sour Gas Susceptibility of an X-80 Steel for Oil and Gas Transport, *Scr. Mater.*, Vol 38 (No. 5), 1998, p 749-755